Defect modeling in spreading nematic droplets

T.-S. Lin, L. Kondic, L. J. Cummings
Department of Mathematical Sciences and Center for Applied Mathematics and Statistics
New Jersey Institute of Technology, Newark, NJ 07102

Experiments by Poulard & Cazabat [1] on spreading droplets of nematic liquid crystal (NLC) reveal a surprisingly rich variety of behavior, including at least two different emerging lengthscales resulting from a contact line instability. In earlier work [2] we modified a lubrication model for nematic liquid crystals due to Ben Amar and Cummings [3], and showed that, in a qualitative sense, it can account for 2D versions of the observed behavior. In the present work we propose a new approach that allows us to explore the effect of anchoring variations on the substrate, again in a 2D geometry. This in turn gives a simple way to model the presence of defects, which are nearly always present in such flows. The new model leads to additional terms in the governing equation. We explore the influence of these additional terms for some simple flow scenarios to gain a basic understanding of their influence.

The coating of a thin film of nematic liquid crystal onto a substrate is one stage in the manufacture of liquid crystal display devices. For example, recent experimental study [4] on coating/filling flows in the nematic phase, was motivated by the search for improved manufacturing techniques of nematic liquid crystal (NLC) microdisplay components. We also refer a reader to a recent popular review article [5] discussing many intriguing features of liquid crystals and to [6, 7] for more in-depth review of liquid crystal phenomenology, including many examples of instabilities particular to liquid crystal flows.

One example of instability involves droplets of NLC spreading on silicon substrate, where the contact line is unstable at high relative humidity (RH $> 60\%$) [1]. In addition, defects always accompany the instabilities. At this stage, however, the role of defects in the instability development is unclear. Whether defects induce the instabilities, are induced by them, or some other explanation altogether, is still an open question. In previous work [2] we presented a model and simulations suggesting that the elastic force arising from the difference between two surface anchoring conditions might be the mechanism of NLC free surface instability. In this Brief Communication we further extend the model to investigate the influence of defects. In the classical theory of liquid crystals (outlined below), defects are represented as jump discontinuities of the molecular orientation field (modeled by the director field). Our approach is to smooth out this discontinuity, so that the director field varies smoothly, but abruptly, in the region of the supposed defect. This makes it possible to explore the coupled defect-flow problem with a smooth continuum model.

The main dependent variables governing NLC dynamics, in the simple two-dimensional case ($\boldsymbol{x} = (x, 0, z)$), are the velocity field $\boldsymbol{v} = (u, 0, w)$ and director field $\boldsymbol{n} = (\sin\theta, 0, \cos\theta)$, the unit vector describing the averaged orientation of the anisotropic axis in the NLC. The director angle θ is determined by minimizing a suitably-defined free energy W within the NLC, with coupling to the flow-field. We use the model of Leslie [8],

$$\frac{\partial}{\partial x_i}\left(\frac{\partial W}{\partial \theta_{x_i}}\right) - \frac{\partial W}{\partial \theta}, \quad -\frac{\partial \pi}{\partial x_i} + \frac{\partial \tilde{t}_{ij}}{\partial x_j} = 0, \quad \frac{\partial v_i}{\partial x_i} = 0, \tag{1}$$

representing energy, momentum, and mass conservation, respectively. Here $\pi = p + W$, where p is the pressure, and W is the elastic energy, which in 2D takes the form

$$2W = K_1(\nabla \cdot \boldsymbol{n})^2 + K_3\big((\boldsymbol{n}\cdot\nabla)\boldsymbol{n}\big)\cdot\big((\boldsymbol{n}\cdot\nabla)\boldsymbol{n}\big),$$

where K_1 and K_3 are elastic constants, taken equal for simplicity: $K_1 = K_3 = K$. $\tilde{t}_{ij}$ is the extrastress tensor (related to the stress t_{ij} by $t_{ij} = -p\delta_{ij} + \tilde{t}_{ij}$), given by

$$\begin{aligned}\tilde{t}_{ij} \;=\; & \alpha_1\, n_k n_p e_{kp} n_i n_j + \alpha_2\, N_i n_j + \alpha_3\, N_j n_i \\ & + \alpha_4\, e_{ij} + \alpha_5\, e_{ik} n_k n_j + \alpha_6\, e_{jk} n_k n_i,\end{aligned}$$

where α_i are constant viscosity coefficients.

Within the framework of the lubrication approximation, the elastic energy W is given (in suitable dimensionless variables [2]) by $2W = K(\theta_z^2 + \delta^2\theta_x^2)/(\delta^2 L^2)$, where $\delta = H/L \ll 1$ is the aspect ratio between a typical drop height H, and the lengthscale of typical variations in the x direction L. Moreover, the velocity field and director field decouple [9]. The energy equation reduces to the Euler-Lagrange equation for minimizing the elastic energy of the film: at leading order, $\theta_{zz} = 0$. Thus,

$$\theta = az + b, \tag{2}$$

where a, b depend only on (x, t) and are determined by the boundary conditions on θ. Note that on the fluid flow timescale, the director "instantaneously" adjusts to the flow, and is thus always in equilibrium for the instantaneous droplet geometry. In addition, for simplicity in the following we have scaled the director angle θ by $\pi/2$, so that $-1 \le \theta \le 1$.

The momentum equations then reduce to a single PDE for $h(x, t)$, the film height, as described in [2, 3, 9]:

$$\frac{\partial h}{\partial t} + \frac{\partial}{\partial x}\left[h^3(\mathcal{C}h_{xxx} - \mathcal{B}h_x) - \mathcal{N}h^3\theta_z\theta_{zx}\right] = 0, \tag{3}$$

where $\mathcal{C} = \delta^3\gamma/(\mu U)$ is an inverse capillary number; $\mathcal{B} = \delta^3\rho g L^2/(\mu U)$ is a Bond number and $\mathcal{N} = K\pi^2/(4\mu U L)$ is an inverse Ericksen number. In these dimensionless groups, γ is the surface tension coefficient, $\mu = \alpha_4/2 > 0$ was chosen as the representative viscosity scaling, U is the typical flow velocity in the plane of the substrate, ρ is the density and g is gravity.

The director field has a preferred orientation at different interfaces. At the free surface (NLC-air interface), the director prefers to align normal to the interface (homeotropic anchoring), while at the flat substrate (NLC-solid interface), the director prefers to align parallel to the surface (planar anchoring). In [3, 9], the cases of strong and weak anchoring (respectively) are considered. However, in [9] the anchoring strength is constant, independent of film thickness and spatial variables. We found [2] that this assumption is not satisfactory in the vicinity of a contact line (strong anchoring is less satisfactory still). In principle, for a relatively thick film the director can accommodate the two preferred angles almost exactly, but for a very thin film it cannot. We introduced an *ad hoc* anchoring condition based on specifying the change in director angle across the film [2],

$$\theta = \theta_0 + \frac{\Theta\, m(h)}{h}\, z. \tag{4}$$

Strong anchoring is imposed on $z = 0$ so that $\theta_0 = \pm 1$, corresponding to planar anchoring. At the free surface $z = h$, the director angle is $\theta_0 + \Theta m(h)$, where Θ is the difference between the preferred anchoring angles at the two interfaces in the bulk flow, and $m(h)$ is a monotone increasing function, approaching zero as $h \to 0$, and approaching 1 as $h \to \infty$. Here, as in [2], we take

$$m(h) = \frac{h^{3/2}}{\beta^{3/2} + h^{3/2}}, \tag{5}$$

where β is a dimensionless anchoring relaxation length. For a film of height $h \ll \beta$ anchoring is weak, and for $h \gg \beta$ it is strong (note that in the limit $\beta \to 0$ we recover the strong anchoring model of [3]). In particular, the functional form (5) has the feature that as $h \to 0$, the nematic term in the governing thin film equation reduces to the same form as the gravity term (see [2] for more details) and leads to droplets that spread faster than the Newtonian equivalents.

In this brief communication we introduce a simple model for defects by assuming that $\Theta = \Theta(x)$ has (smoothed) jumps at specific positions. Figure 1 shows two possible defect configurations: a point defect and a line defect. In our asymptotic model, to leading order the two are essentially equivalent [10].

Since defects are often associated with inhomogeneities of the substrate, we assume that these points are fixed, ie., not moving with the flow. The chosen implemented single defect formulation is

$$\Theta(x) = \tanh\left(\frac{x - x_0}{w}\right), \tag{6}$$

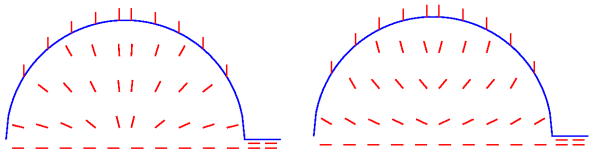

(a)Point defect. (b)Line defect.

FIG. 1: Two different possible defects within a droplet (represented by the solid curve). The short lines represent the local orientation of the director field.

where x_0 is the position and w is the effective width of the defect, determined in practice by the ratio between the typical width of point defect and the spatial lengthscale. In our numerical simulations we choose $w = 0.1$. Multiple defects, which are often observed, can be modeled by replacing Eq. (6) by a superposition of hyperbolic tangent functions.

Finally, by combining the evolution equation, Eq. (3), with the director field, Eq. (4), we obtain the governing PDE as

$$\frac{\partial h}{\partial t} + \frac{\partial}{\partial x}\left[h^3(\mathcal{C}h_{xxx} - \mathcal{B}h_x) + \mathcal{N}\Theta^2(m^2 h_x - hmm_x) - \mathcal{N}\Theta\Theta_x m^2 h\right] = 0, \tag{7}$$

where the anchoring function, $m(h)$, and the function $\Theta(x)$, specifying the defect(s), are defined in Eqs. (5, 6).

The evolution equations similar in structure to Eq. (7) have been extensively used in modeling a variety of problems relevant to thin-film dynamics [11]. In our case, Eq. (7) contains five parameters, $\mathcal{C}, \mathcal{B}, \mathcal{N}, \beta, h_0$ and, in the case with defects, the defect location(s) and width also. It is hard in general to explore the solutions in such a large parameter space. In the following, we fix the capillary length as the characteristic lengthscale, $L = \sqrt{\gamma/\rho g}$, which is equivalent to $\mathcal{C} = \mathcal{B}$. We further assign $\mathcal{C} = \mathcal{B} = 1$, and investigate the effect of $\mathcal{N}$, β and of defects.

We first summarize the results of the classic linear stability analysis (LSA) of a flat film solution of the defect-free model, $\Theta(x) = 1$, given in [2]. Expanding $h(x,t) = h_0 + \epsilon h_1(x,t) + \cdots$, where $0 < \epsilon \ll 1$, and assuming $h_1 = h_{10}\exp(ikx - \omega t)$, we obtain the dispersion relation

$$\omega = -h_0^3 k^2\left(k^2 + (1 - \mathcal{N}M(h_0,\beta))\right),$$
$$M(h_0,\beta) = \frac{h_0^{3/2} - \frac{\beta^{3/2}}{2}}{(h_0^{3/2} + \beta^{3/2})^3}.$$

The flat film is unstable to sufficiently long-wavelength perturbations if $\mathcal{N}M(h_0,\beta) > 1$. Perturbations with wavenumbers $k \in (0, k_c)$ are then unstable, where $k_c = \sqrt{\mathcal{N}M(h_0,\beta) - 1}$; and the fastest-growing wavenumber is $k_m = \sqrt{(\mathcal{N}M(h_0,\beta) - 1)/2}$.

Figure 2 shows the stability diagram for $\mathcal{N} = 50$ in β-h_0 space. The region enclosed by the solid curve indicates

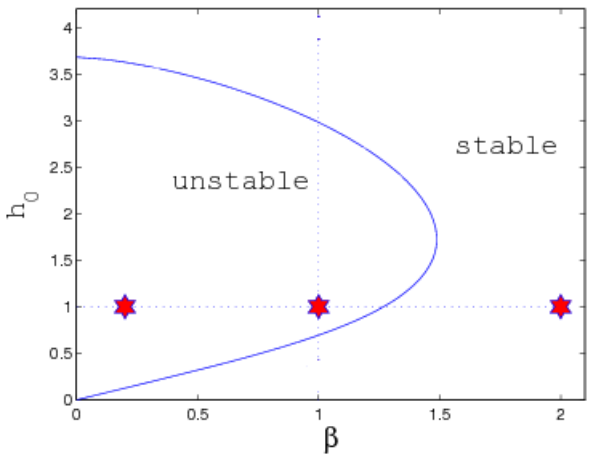

FIG. 2: Stability diagram in (β, h_0)-space for $\mathcal{N} = 50$. The region enclosed by the solid (blue) curve represents unstable solutions. (Red) stars point the parameters considered in Figs. 3, 4,and 5.

the unstable part. The stars correspond to the numerical simulations presented in the following paragraphs. Note that, in the absence of defects, a flat film is more unstable when β is smaller. This is not surprising: recalling that β is the dimensionless relaxation length, smaller β means larger free surface anchoring strength and higher elastic forces within the film. In particular, in the strong anchoring limit, $\beta = 0$, thick films are stable while all thin films are unstable.

Figures 3, 4, and 5 show numerical simulations of spreading droplets with and without defects for different chosen parameter values (marked by stars in Fig. 2). The solid curve shows the droplet profile, h, while the dashed curve shows the corresponding anchoring function, measured by $\Theta(x)\, m(h)$. The initial conditions are shown by dash-dotted lines in part (a) of each figure.

Figure 3 shows a stable spreading scenario ($\mathcal{N} = 50$, $\beta = 2$, $h_0 = 1$). Figure 3(a) shows the numerical result at $t = 100$ with no defects, $\Theta(x) \equiv 1$; and Fig. 3(b), shows the result at the same time with three defects at $x = -5$, 0 and 7. As is evident, there is no free surface instability in this case, which is consistent with the LSA (even though the LSA is valid only for flat film, it is still a good indicator for the spreading surface instabilities). On the other hand, in Fig. 3(b) there are small crests right at the location where the defects are imposed [12]. These crests appear to be a robust feature of our simulations with defects. Note the abrupt change in sign of the anchoring function $\Theta(x)m(h)$ as we pass through a defect, corresponding to the abrupt change in the anchoring angle.

Figure 4 shows an unstable spreading scenario ($\mathcal{N} = 50$, $\beta = 1$, $h_0 = 1$). In the early stages, the drop evolves from a square profile ($t = 0$, dash-dotted line in Fig. 4(a)) into a drop with two humps (Fig. 4(a): $t = 1$). As the drop spreads, these two humps merge into one and eventually disappear (Fig. 4(c): $t = 100$). Parts (b) and (d) of Fig. 4 show the case with a defect at $x = 3$. The main difference between this and the defect-free case is that the hump is now pinned at the location of the defect, instead of symmetrically at the center. So in Fig. 4(b), the hump on the left merges with that on the right and in Fig. 4(d), the location of the hump is coincident with the location of the defect.

Figure 5 shows the case of an unstable non-spreading

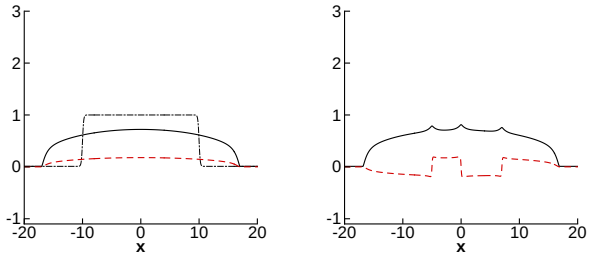

(a)$t = 100$, no defects. (b)$t = 100$, with defects at $x = -5$, 0 and 7.

FIG. 3: Simulations with $h_0 = 1$, $\beta = 2$, $\mathcal{N} = 50$. The solid curves show the droplet profile, h, the (red) dashed curves show the corresponding anchoring function, measured by $\Theta(x)\, m(h)$, and the initial conditions are shown by dash-dotted lines in part (a).

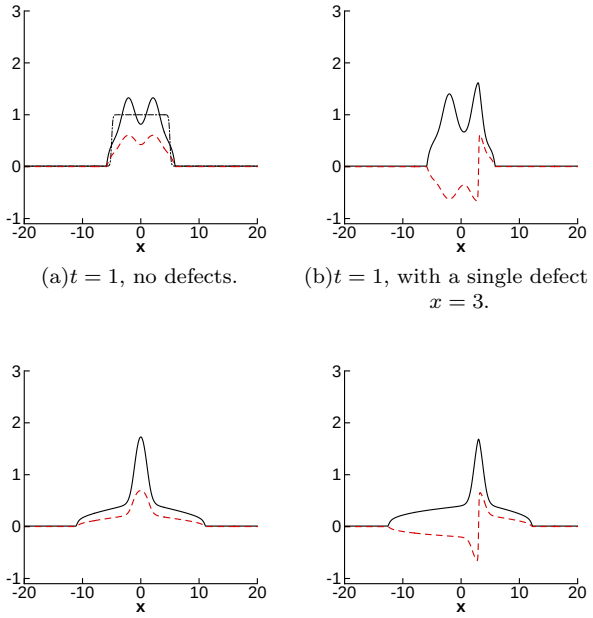

(a)$t = 1$, no defects. (b)$t = 1$, with a single defect at $x = 3$.

(c)$t = 100$, no defects. (d)$t = 100$, with a single defect at $x = 3$.

FIG. 4: Simulations with $h_0 = 1$, $\beta = 1$, $\mathcal{N} = 50$. The line patterns are as in Fig. 3.

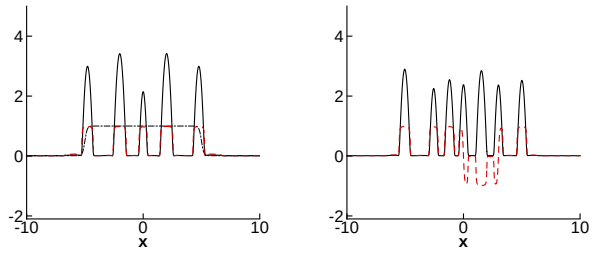

(a)$t = 5$, no defects. (b)$t = 5$, with defects at $x = 0$, 3.

FIG. 5: Simulations with $h_0 = 1$, $\beta = 0.2$, $\mathcal{N} = 50$. The line patterns are as in Fig. 3.

droplet, as discussed in [2] ($\mathcal{C} = 50$, $\beta = 0.2$, $h_0 = 1$). Even without defects, Fig. 5(a), the initial profile breaks into several distinct humps, which do not spread. For the case with two prescribed defects, Fig. 5(b), two additional humps appear right at the defect locations.

In all our simulations (more than are shown here) we find that the defects do not appear to alter the stability of the bulk droplet. For a stable spreading droplet, a defect leads to a crest in the profile at large times, while for the unstable case, the defect gives rise to a pinned hump. Furthermore, in either case defects do not influence spreading versus non-spreading behavior. This is because defects are localized effects. The global effects, such as surface anchoring strength over the whole droplet, are more likely to affect the spreading behavior.

In this work we have shown examples of stable spreading, unstable spreading and unstable non-spreading droplets (as characterized in [2]), with and without defects. We note that, as there are five parameters in our defect-free model ($\mathcal{C}$, $\mathcal{B}$, $\mathcal{N}$, β, h_0), it is in principle possible to modify stability/instability by varying any of the parameters. However, for simplicity, in this paper we have shows only cases in which β is varied, with all other parameters fixed, and investigated the effect of defects on the evolution. We have examined other possibilities not shown here, and have found similar qualitative behavior.

In conclusion, we have presented a new model for spreading of a thin film of nematic liquid crystal that allows anchoring strength to relax as the film height goes to zero, and that can also account for the presence of defects. Simple linear stability analysis for a flat film appears to serve as a good indicator of the behavior of more complicated spreading drops. In particular, the presence of defects does not appear to alter the stability characteristics. While we are still some way from quantitative simulations of the experimental results of Poulard & Cazabat [1], the 2D model presented here can exhibit the key experimental features of stable spreading, unstable spreading and arrested instability. We believe it to be a good starting-point for a full theoretical description of spreading nematic droplets. Simulations on a more realistic model for three-dimensional spreading, in which point defects can be accurately represented, are underway.

Acknowledgements This work was supported by the NSF under grant DMS-0908158.

[1] C. Poulard, A. M. Cazabat, "Spontaneous spreading of nematic liquid crystals," *Langmuir* **21**, 6270 (2005).

[2] L. J. Cummings, T.-S. Lin, L. Kondic, "Modeling and simulations of the spreading and destabilization of nematic droplets," *Phys. Fluids* **23**, 043102 (2011).

[3] M. Ben Amar, L. J. Cummings, "Fingering instabilities in driven thin nematic films," *Phys. Fluids* **13**, 1160 (2001).

[4] D. W. Calton, K. Seunarine, G. Bodammer, I. Underwood, "Liquid crystal flow control using microfabrication techniques," *IEE Proc. Optoelectron.* **147**, 163 (2000).

[5] P. Palffy-Muhoray, "The diverse world of liquid crystals," *Phys. Today* **Sep.**, 54 (2007).

[6] P. G. De Gennes, J. Prost, "The physics of liquid crystals," *Oxford University Press*, USA, (1995).

[7] S. Chandrasekhar, "Liquid crystals," *Combridge University Press*, 2nd edition, (1993).

[8] F. M. Leslie, "Theory of flow phenomena in liquid crystals," *Adv. Liquid Crystals* **4**, 1 (1979).

[9] L. J. Cummings, "Evolution of a thin film of nematic liquid crystal with anisotropic surface energy," *Europ. J. Appl. Math.* **15** (6), 651 (2004).

[10] As shown in Eq. (4), the director angle θ is a linear function in z. It is clear that an idealized line defect, away from the actual discontinuity, has director angle that is linear in z (the sign of the linear multiplier simply changes as we cross the discontinuity). The director angle near an idealized point defect at $x^* = 0 = z^*$ on the other hand (scaled by $\pi/2$ as described in the text) is described locally by a function of the form $\theta \approx \pm(2/\pi)\tan^{-1}(x^*/z^*)$ (in dimensional coordinates (x^*, z^*)). Whether the sign is $(+)$ or $(-)$ here is immaterial since θ is defined only modulo π and we choose $(-)$ for convenience. At a fixed horizontal distance x_0^*, and in the region $z^* \ll x_0^*$ this is approximated by $\theta \approx \mp 1 + 2z^*/(\pi x_0^*)$. Hence for films thinner than the defect core, the above linear approximation (in which the sign of the linear multiplier again changes as the defect is crossed and x_0^* changes sign) is valid everywhere outside the core. For sufficiently thin films therefore, point and line defects may be considered equivalent outside some core. In reality, a line defect is associated with higher elastic energy than a point defect, so line defects tend to be unstable and are less likely to be observed.

[11] R. V. Craster, O. K. Matar, "Dynamics and stability of thin liquid films," *Rev. Mod. Phys.* **81**, 1131 (2009).

[12] R. B. Meyer, "Point disclinations at a nematic-isotropic liquid interface," *Mol. Cryst. Liq. Cryst.* **16**, 355 (1972).